energies

MDPI

Article

Application of Shallow-Hole Blasting in Improving the Stability of Gob-Side Retaining Entry in Deep Mines: A Case Study

Yong Chen [1], Shuqi Ma [1,2,*], Yugui Yang [3], Ningkang Meng [1] and Jianbiao Bai [1]

[1] State Key Laboratory of Coal Resource and Safe Mining, China University of Mining and Technology, Xuzhou 221008, China; chenyong@cumt.edu.cn (Y.C.); mengnk@cumt.edu.cn (N.M.); baijianbiao@cumt.edu.cn (J.B.)

[2] Key Laboratory of Transportation Tunnel Engineering, Ministry of Education, Southwest Jiaotong University, Chengdu 610031, China

[3] State Key Laboratory for Geomechanics and Deep Underground Engineering; China University of Mining and Technology, Xuzhou 221008, China; yuguiyang@126.com

* Correspondence: shuqima.ma@gmail.com

Received: 29 August 2019; Accepted: 20 September 2019; Published: 23 September 2019

Abstract: The hanging of hard roof strata in the gob-side retaining entry in deep mines could lead to dynamic disasters. The pressure relief mechanism for the hard roof strata using shallow-hole blasting was investigated by a combined method of theoretical analysis, numerical simulation, and field test in the Sanhejian coal mine. The shallow-hole blasting model was established using LS-DYNA3D (Livemore software of explicit dynamics analysis code). The evolution and propagation law of effective stress induced by shallow-hole blasting was analyzed. The parameters related to shallow-hole blasting were determined via a combined method of numerical analysis and theoretical calculations. These were applied to the field tests. The effect of shallow-hole blasting on the strata control of deep gob-side retaining entry was studied by comparing two scenarios in the field: a deep gob-side retaining entry with and without shallow-hole blasting. It was found that the convergences of the entry decreased due to the shallow-hole blasting. This indicates that shallow-hole blasting is a good technique to maintain the stability of the gob-side retaining entry with a hard roof in deep mines.

Keywords: gob-side entry retaining; deep mine; shallow-hole blasting; hard roof

1. Introduction

Gob-side retaining entry is widely used in China due to its various advantages of increasing recovery rate, reducing tunneling rate, reducing roadway maintenance cost, solving corner gas overrun, and increasing mining economic benefits. The gob-side retaining entry technology is now mature for simple geology conditions [1–5] and was also applied in underground mines with a thick coal seam where the fully mechanized top coal caving method is used [6–10]. The application of the gob-side retaining entry technique to deep mines with competent roof strata is, however, still a challenge. Roadway layouts with a long distance and large section are often adopted in large modern coal mines due to the large production rate and large equipment used in these mines. The length of the gob-side retaining entry in large modern coal mines often exceeds 1 km and sometimes reaches up to 3 km. The surrounding rock mass is strongly influenced by mining induced dynamic pressure. The roadway section is squeezed sharply, often leaving less than 50% of the original size, which cannot fulfill the requirement of ventilation. Some roadways encounter extremely large deformation, and the gob-side retaining entry cannot be implemented to achieve the coal and gas extraction [11].

The implementation of gob-side retaining entry in deep colliery is a technical problem due to the large mining-induced stress.

The gob-side retaining entry in deep colliery is subjected to the superposition of high initial in situ stress and strong mining-induced stress, which makes it very difficult to maintain the stability of the gob-side retaining entry in deep colliery. It becomes even more difficult for the gob-side retaining entry with hard and competent roof strata. A large area of roof strata will hang for a long time over the goaf area, which will impose large pressure on the backfill body and lead to large deformation and eventually collapse of the backfill body. In addition, the breakage of the hanging roof strata can cause large areas of roof weighting and strong winds, which might severely affect the mine safety and productivity [12–15]. Therefore, measures should be taken to reduce the effects of the hanging hard roof strata.

The current common measure is to change mechanical conditions of gob-side retaining entry by weakening the roof strata strength, relieving the roof pressure, and optimizing the way the roof strata breaks. The used technologies are deep-hole and shallow-hole blasting, water injection to soften rock mass, hydraulic fracture to weaken rock mass, etc. Among them, the most commonly used technologies to relieve roof pressure are deep-hole and shallow-hole blasting technology [16–18]. Deep-hole pre-splitting blasting is mainly applied to the roadways or the working face, and blasting parameters are mostly obtained using numerical analysis and laboratory experiments. However, the shallow-hole blasting technique is seldom applied to gob-side retaining entry, and the mechanism of the shallow-hole blasting technique should be analyzed systematically.

This paper presents a case study on the mechanism of shallow-hole blasting technology for gob-side retaining entry with a hard roof through a combined method of theoretical calculation, numerical analysis, and field test. This study was conducted on gob-side retaining entry with a hard roof in the Sanhejian deep coal mine of Jiangsu Mining Group. This paper presents the determination of key parameters used in shallow-hole blasting. The outcomes of this study will help improve the stability of gob-side retaining entry with hard roof strata and guarantee the safety and productivity of colliery.

2. Geological Conditions

The Sanhejian mine of the Jiangsu Mining Group is located in Xuzhou, east of China. The 72207 working face is located in the south second panel of the well field, with the depth varying from –900 to –1050 m. The main mining coal seam is #7 coal seam. The width and the strike length of the working face are 180 and 820 m, respectively. The gob-side retaining entry, as shown in Figure 1, started 670 m away from the stop line of the 72207 working face. The retaining entry is used as the transportation entry of the 72209 working face.

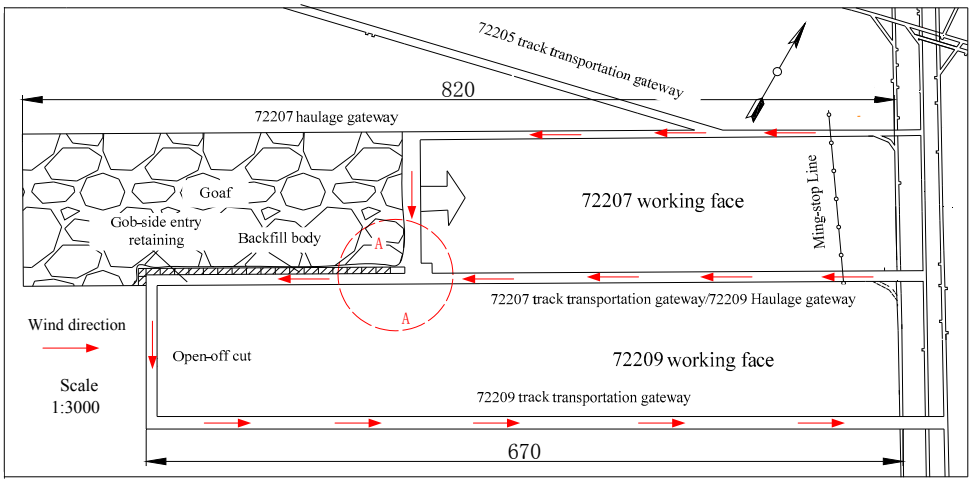

(**a**)

Figure 1. *Cont.*

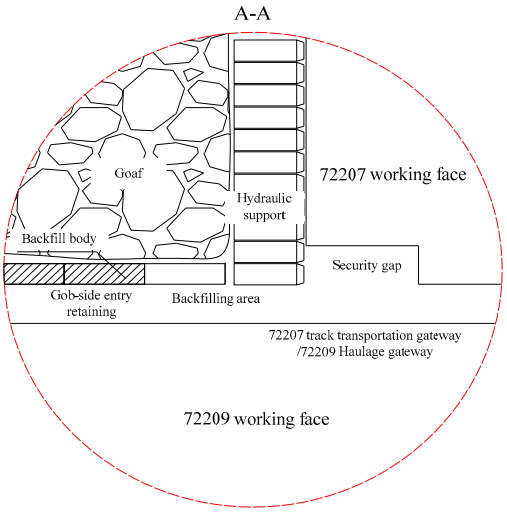

(**b**)

Figure 1. The plane view of the 72207 working face. (**a**) Schematic diagram of 72207 working face (**b**) A-A Profile.

The #7 coal is a black brittle, fragile, and semi-black briquette. The coal thickness in the 72207 working face varies little, with an average of 2.4 m. The average dip angle is 17°, the gas content is 0.082–0.41 cm^3/g, and the ground temperature is 31–37 °C. The direct roof in the 72207 working face is 1.0-m-thick mudstone, the main roof is fine sandstone with an average thickness of 6.8 m, and the direct floor is 15.37-m-thick mudstone. The lithologic information of the 72207 working face is shown in Figure 2.

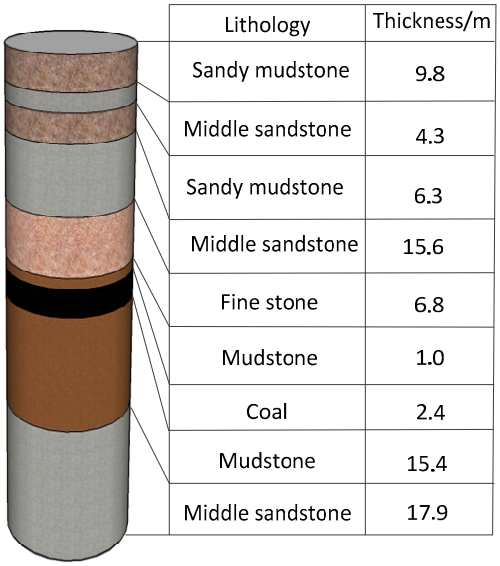

Lithology	Thickness/m
Sandy mudstone	9.8
Middle sandstone	4.3
Sandy mudstone	6.3
Middle sandstone	15.6
Fine stone	6.8
Mudstone	1.0
Coal	2.4
Mudstone	15.4
Middle sandstone	17.9

Figure 2. The lithologic information of the 72207 working face.

Laboratory tests were carried out to obtain the mechanical properties of coal samples and rock samples from the roof and floor of the 72207 working face in the State Key Laboratory of Coal Resources and Safety Mining, China University of Mining and Technology. The results of coal, roof, and floor samples are shown in Table 1.

Table 1. Experimental parameters of rock and rock mechanics.

Sample Name	Sample Number	Sample Size: Diameter (mm) × Height (mm)	Uniaxial Compressive Strength (MPa)	Uniaxial Tensile Strength (MPa)	Cohesion (MPa)	Internal Friction Angle (°)
Main roof	1-1-1	49.86 × 101.26	65.43	5.86	7.7	42
	1-1-2	50.20 × 100.30				
	1-1-3	50.00 × 101.20				
Immediate roof	2-1-1	49.58 × 101.56	33.65	4.475	2.51	40
	2-1-2	49.20 × 100.36				
	2-1-3	49.30 × 100.46				
#7 coal	3-1-1	50.60 × 102.34	8.82	2.17	2.0	26.72
	3-1-2	50.08 × 100.20				
	3-1-3	50.20 × 100.30				
Floor	4-1-1	49.86 × 102.36	40.6	6.986	2.8	46.46
	4-1-2	50.20 × 101.14				
	4-1-3	50.10 × 101.20				

According to the classification of rock mechanical properties in China, the main roof of the 72207 working face, which is characterized by high strength, large thickness, high integrity, and undeveloped joints, is classified as a hard roof (Table 2) [12]. A large hanging roof can easily occur during the mining process. The hanging roof strata will break and cave into the gob upon reaching the limit hanging span due to the advancement of the working face. The hanging roof caving will cause intense dynamic pressure and lead to severe deformation of entry.

Table 2. The classification of mechanical properties on coal-rock mass.

Sample Name	Hard (>60 MPa)	Harder (60–30 MPa)	Softer (30–15 MPa)	Soft (15–5 MPa)
Main roof	√	-	-	-
Immediate roof	-	√	-	-
#7 coal	-	-	-	√
Floor	-	√	-	-

3. Mechanism of Gob-Side Entry Retaining Weighting of Deep Hard Roof

3.1. Mechanism of Gob-Side Entry Retaining Weighting of Hard Roof

The hard roof strata of the 72207 working face should remain intact and hang above the gob. With the advancement of the 72207 working face, the size of the hanging area will increase. The roof strata will bend and subside when the hanging area reaches a certain value, imposing large pressure on the roadside backfill body and the surrounding rock mass. The gob-side retaining entry would be subject to large deformation and might be closed. The safety of the retaining entry cannot be guaranteed. The roof strata will break and cave in the gob area when the area of the hanging roof strata exceeds the limit value, causing severe dynamic pressure. The hanging roof strata and large pressure primarily occur in thick and hard roof strata. The evolution of large pressure in the hard roof strata is shown in Figure 3.

In order to avoid the large deformation of the retaining entry and other dynamic disasters, measures such as deep-hole pre-splitting blasting and shallow-hole circulation blasting should be taken to weaken the hard roof strata. The length of the drilling hole for deep-hole pre-splitting blasting is usually larger than 20 m, and the drilling process is complex. Shallow-hole blasting is applicable in mines having a low gas content. Shallow-hole blasting is carried out in the gob-side temporary supporting area to form the pre-splitting line in the roof. The immediate roof will break and fall firstly. Afterward, the main roof will break and cave into the gob along the pre-splitting line (Figure 4b). The principle of shallow-hole blasting is to reduce the integrity of the hard roof in the gob side and to enable a certain height of roof strata to break and cave into the gob. With the advancement of the working face, the overlying roof strata will break along the pre-splitting line and the backfill body will support the remaining roof strata. This will ensure the stability of the roof strata above the retaining entry and reduce the pressure on the roof strata above the retaining entry. The retaining entry can be

well retained, and it can be used to serve as the next working face. UDEC (Universal Distinct Element Code) was used to demonstrate the behavior of overlying roof strata before and after shallow-hole blasting (Figure 4).

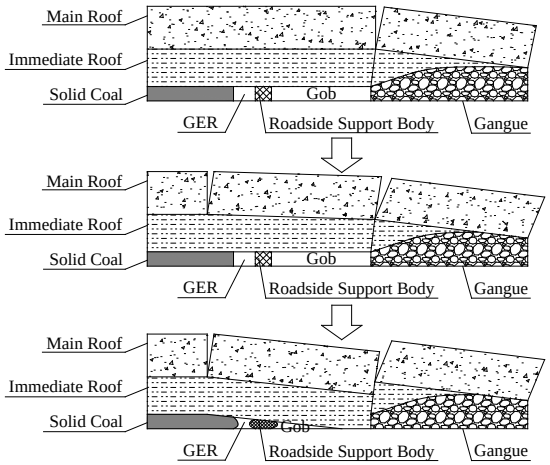

Figure 3. The evolution of large pressure in the hard roof strata. GER: gob-side entry retaining.

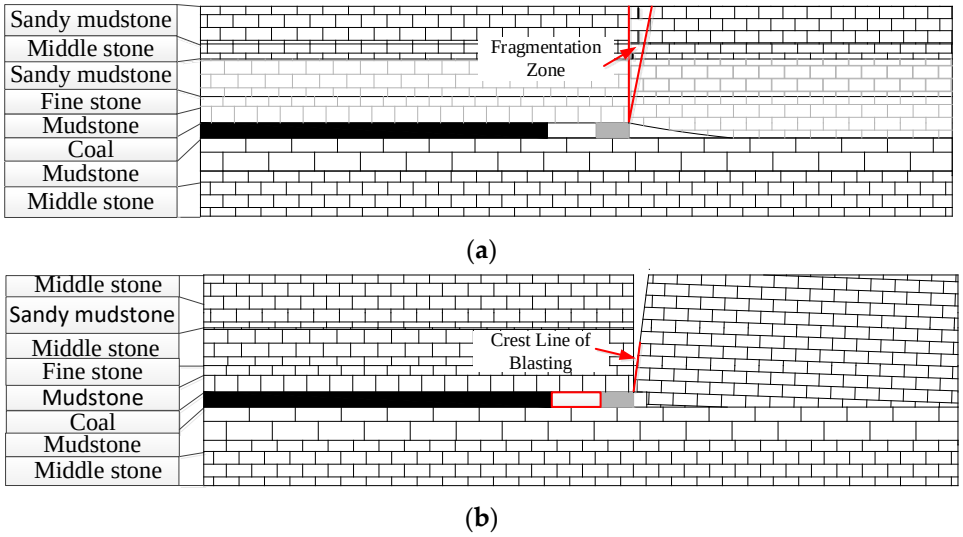

Figure 4. The behaviors of overlying roof strata with and without shallow-hole blasting. (**a**) Roadway retained surrounding rock structure when roof is not cut; (**b**) roadway retained surrounding rock structure after roof cutting.

3.2. Determination of Critical Parameters for Shallow Blasting

3.2.1. Shallow-Hole Blasting Range Law

The immediate roof is strongly influenced by the blasting-induced dynamic impacts. The roof rock can be classified into a crushing zone (I), crack zone (II), and elastic deformation zone (III), based on the degree of damage of the rock due to the blasting. Figure 5 schematically shows the classification of roof rock caused by the shallow-hole blasting. A detailed discussion on the classification of roof rock is also presented below [19–22].

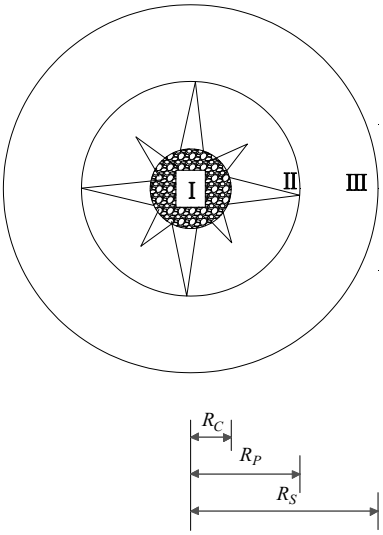

Figure 5. Zone characteristics of shallow-hole blasting.

(I) Crushing zone

The explosive energy is partially consumed by the compression or crushing of the rock, forming a crushing zone near the borehole (I zone in Figure 5). Under uncoupled charge conditions, the radius of the crushing zone can be calculated as follows:

$$R_C = \left(\frac{\rho_m {C_P}^2}{5\sigma_c}\right)^{\frac{1}{2}} \left(\frac{\frac{\rho_0 {D_C}^2}{8}}{\sigma_c A}\right)^{\frac{1}{4}} r_0 \tag{1}$$

where ρ_0 is the explosive density (kg/m^3), D_C is the explosive detonation velocity (m/s), σ_c is the rock uniaxial compressive strength (MPa), r_0 is the radius of the blast hole (m), A $= \left(\frac{\rho_m {C_P}^2}{\sigma_c}\right)^{1/4}$, and ρ_m and C_P are the the rock density (kg/m^3) and the longitudinal wave velocity (m/s).

(II) Rupture zone

As the propagation range of stress waves increases, the energy density per unit area of rock decreases. The stress wave is propagated away from the crushing zone. If the maximum tensile stress is larger than the dynamic tensile strength of the rock, cracks would accordingly occur and the rupture (crack) zone is formed (II zone in Figure 5). The radius of the crack zone can be calculated as follows:

$$R_P = \left[\frac{\nu \rho_0 {D_C}^2}{8\sigma_t(1-\nu)}\right]^{\frac{1}{(2-\frac{\nu}{1-\nu})}} r_0 \tag{2}$$

where ν is the Poisson's ratio of the rock, and σ_t is the rock uniaxial tensile strength (MPa).

(III) Elastic deformation zone

The stress waves are further decreased when propagating further away from the borehole. The decreased dynamic stress cannot cause fracture of the rock and can only induce elastic deformation (III zone in Figure 5). The radius of the elastic deformation zone can be calculated by

$$R_S = (1.5 - 2.0)\sqrt[3]{Q} \tag{3}$$

where Q is the quality of explosives for a single hole (kg).

According to the used explosives and blast-hole parameters, the geology conditions in the 72207 working face in the Sanhejian colliery were determined as ρ_0 = 1200 kg/m^3, D_C = 3600 m/s, σ_c = 65.43 MPa, γ_0 = 2.1 × 10^{-2} m, ρ_m = 2.7 × 10^3 kg/m^3, C_p = 3000 m/s, ν = 0.22, σ_t = 5.8 MPa,

and Q = 2.4 kg. The above parameters were substituted into Equations (1)–(3), and the radius of the crushing zone was calculated to be 0.29 m, the radius of the crack zone was found to be 0.34 m, and the radius of the elastic zone was determined to be 2.0–2.68 m.

3.2.2. Determination of Critical Parameters for Shallow Blasting

(1) Blasting depth of shallow-hole blasting

The depth of the blasting hole influences the effects of blasting on weakening the roof strata and eventual roof strata caving [23]. The blasting hole depth was determined by Equation (4) according to the geological conditions of the 72207 working face in the Sanhejian colliery. The average thickness of the immediate roof of the 72207 working face is 1.0 m. The average thicknesses of the main roof and coal seam are 6.8 m and 2.4 m.

$$H = \frac{M}{K_P - 1} \tag{4}$$

where H is the hole depth (m), M is the mining height (m), and K_P is the rock's expansion coefficient.

The mining height M = 2.4 m and the rock's expansion coefficient K_P = 1.5 were substituted into Equation (4), giving H = 4.8 m. Based on the theoretical analysis and the author's field experience, the design hole depth was selected as 5.0 m in order to achieve the designed blasting effects. The inclination angle to the gob side of 10° was selected to facilitate the drilling process and the subsequent roof strata caving.

(2) Explosive parameters of shallow-hole Blasting

According to the China Coal Mine Safety Regulations [24], the second-grade permissible explosive for the mining industry was selected for the shallow-hole blasting in the 72207 face, as Sanhejian colliery is characterized as a low-gas mine. The explosive density and the detonation wave propagation velocity have direct impacts on the blasting effect. The second-grade permissible explosive cartridge has a length of 300 mm, a diameter of 27 mm, and a weight of 0.3 kg per block, with a detonation rate of 3600 m/s and a density of 1200 kg/m^3. Each cumulative energy tube is 1.4 m long and can contain four explosive cartridges. A detonator is installed in the last explosive cartridge for each cumulative energy tube.

To facilitate the installation of the explosives, the inner diameter of the cumulative energy tube is required to be larger than the diameter of the explosive cartridge, and the outer diameter of the cumulative energy tube should be smaller than the diameter of the borehole. Boreholes of 42 mm in diameter were drilled in the roof strata. The diameter of the explosive cartridge was 27 mm. Hence, the cumulative energy tubes with an outer diameter of 32 mm and an inner diameter of 29 mm were used.

(3) The spacing between the shallow blasting boreholes

Numerical analysis using the nonlinear dynamic analysis software LS-DYNA was carried out to analyze the influences of the borehole spacing on the blasting effects. The ALE (Arbitrary-Lagrangian-Eulerian) method and multi-material fluid–solid coupling method were adopted when establishing the numerical model [25]. The measuring points were set in the middle point of the two holes to monitor the variation of the effective stress within the rock. The model size was 6000 mm × 5000 mm × 5000 mm, the hole diameter was 42 mm, the diameter of the explosive cartridge was 27 mm, and the depth of the hole was 5000 mm, as shown in Figure 6.

The JWL (Jones-Wilkens-Lee) equation was adopted in LS-DYNA3D to describe the relationship between the pressure applied to the borehole wall by a unit detonation product and the volume of the detonation product (Equation (5)).

$$P = A\left(1 - \frac{\omega}{R_1 V}\right)e^{-R_1 V} + B\left(1 - \frac{\omega}{R_2 V}\right)e^{-R_2 V} + \frac{\omega E_0}{V} \tag{5}$$

where P is the explosive detonation unit pressure (MPa), E_0 is the explosive detonation product initial density, V is the explosion detonation product relative volume, and A, B, R_1, R_2, and ω are explosive material constants determined from the experiment, as shown in Table 3.

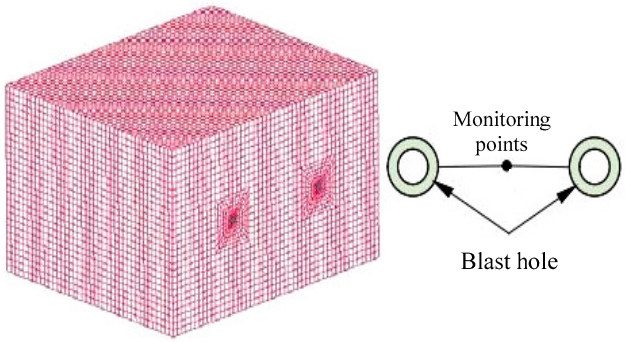

Figure 6. Numerical model of the shallow-hole blasting.

Explosive parameters and JWL equation parameters are given in Table 3. The rock material model adopts the kinematics hardening plastic model. The rock mechanical parameters used in the numerical analysis are shown in Table 4.

Table 3. Parameters of the explosives and JWL equation.

Explosive Density (kg/m^3)	Explosive Detonation (m/s)	A (GPa)	B (GPa)	E_0 (GPa)	R_1	R_2	ω
1200	3600	214.4	0.182	4.192	4.2	0.9	0.15

Table 4. Physico-mechanical parameters of rock in the numerical model.

Density (kg/m^3)	Shear Modulus (GPa)	Bulk Modulus (GPa)	Poisson's Ratio	Yield Strength (MPa)	Cohesion (MPa)	Internal Friction Angle (°)	Dynamic Tensile Strength (MPa)
2700	10.5	15	0.22	90	7.7	42	18

The effects of the borehole spacing

The effective stress curve at the monitoring points was obtained for different hole spacings of 0.8 m, 1.0 m, and 1.2 m using the post-processing module LS-PREPOST (Livemore software of pre and post-processor in LS-DYNA, as shown in Figure 7.

The following can be seen from Figure 7:

(1) The increase in hole spacing decreased the effective stress. A smaller hole spacing led to a greater effective stress peak at the monitoring point. The peak effective stresses for the hole spacings of 0.8, 1.0, and 1.2 m were 78.3, 49.5, and 44.7 MPa, respectively.

(2) The effective stress reduced with time and tended to become stable around a certain value, which decreased with the increase in hole spacing. The stable effective stresses for the hole spacings of 0.8, 1.0, and 1.2 m were 45, 20, and 10–20 MPa, respectively.

(3) The rock breaks when the stable effective stress is greater than the dynamic tensile stress of the rock. The stable effective stresses generated when the hole spacings were 0.8 and 1.0 m were greater than the dynamic tensile strength of the rock. When the hole spacing was 1.2 m, the effective stress was less than the dynamic tensile strength of the rock. Thus, the spacing of the blasting holes was determined as 1.0 m.

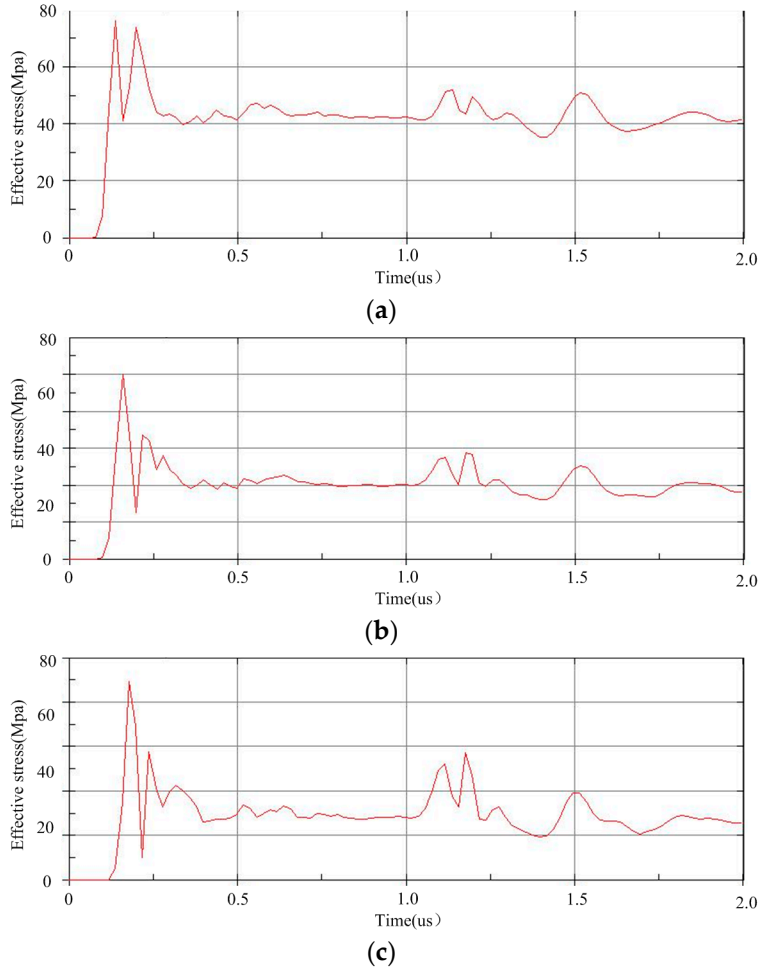

Figure 7. Effective stress curves of monitoring point for different blasting hole spacings: (**a**) borehole spacing of 0.8 m; (**b**) borehole spacing of 1.0 m; (**c**) borehole spacing of 1.2 m.

The evolution of the effective stress in shallow-hole blasting

The evolution of the effective stress in the rock at the hole spacing of 1.0 m is shown in Figure 8.

It can be seen from Figure 8 that, when the blasting time was 39.886 μs (Figure 8a), the range of the explosive stress wave reached 138 mm. The stress wave propagated in the rock mass with time, and the stress waves of the adjacent holes met and overlapped in the middle point at 139.84 μs. The stress superposition at the middle point increased with time, and the effective stress reached the maximum value of 49.5 MPa at 299.51 μs, which exceeds the dynamic tensile strength of 18 MPa. The stress superposition effect decreased, and the effective stress reduced to 20 MPa, which is still larger than the dynamic tensile strength of the roof strata.

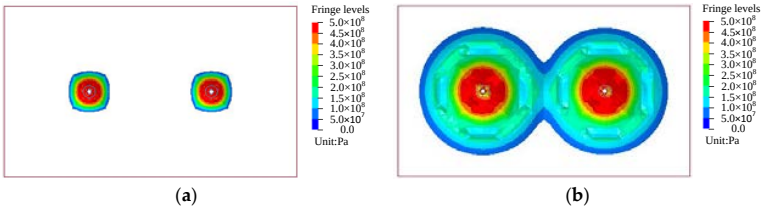

Figure 8. *Cont.*

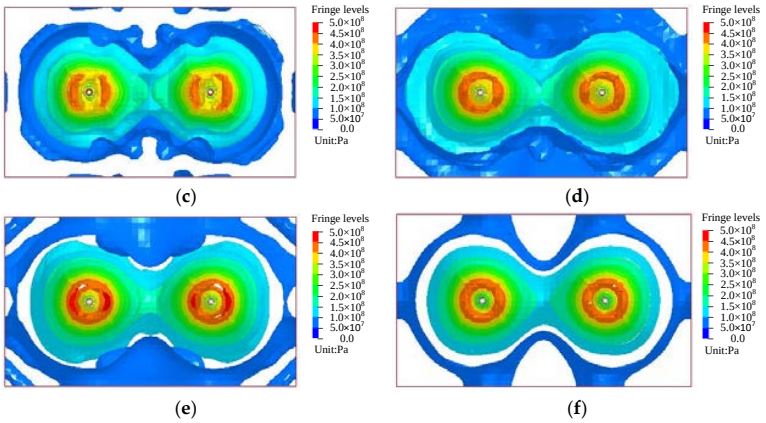

Figure 8. The evolution of the effective stress in the rock at the hole spacing of 1.0 m: (**a**) 39.886 μs; (**b**) 139.84 μs; (**c**) 299.51 μs; (**d**) 619.09 μs; (**e**) 1039.5 μs; (**f**) 1999.9 μs.

4. Engineering Application

4.1. Roadway Support

4.1.1. Roadway Primary Support

The roadway in the 72207 working face has a width of 4500 mm and a centerline height of 2600 mm. The support arrangement for the roadway in the 72207 working face is schematically shown in Figure 9. Rock bolts of 22 mm in diameter and 2000 mm in length and cable bolts of 18.9 mm in diameter and 5200 mm in length were installed to support the roof strata. The rock bolts used for the rib support of the roadway were 20 mm in diameter and 2000 mm long. Additional cables of 18.9 mm in diameter and 5200 mm in length were installed in the roof strata at the backfill body side at a spacing of 1200 mm.

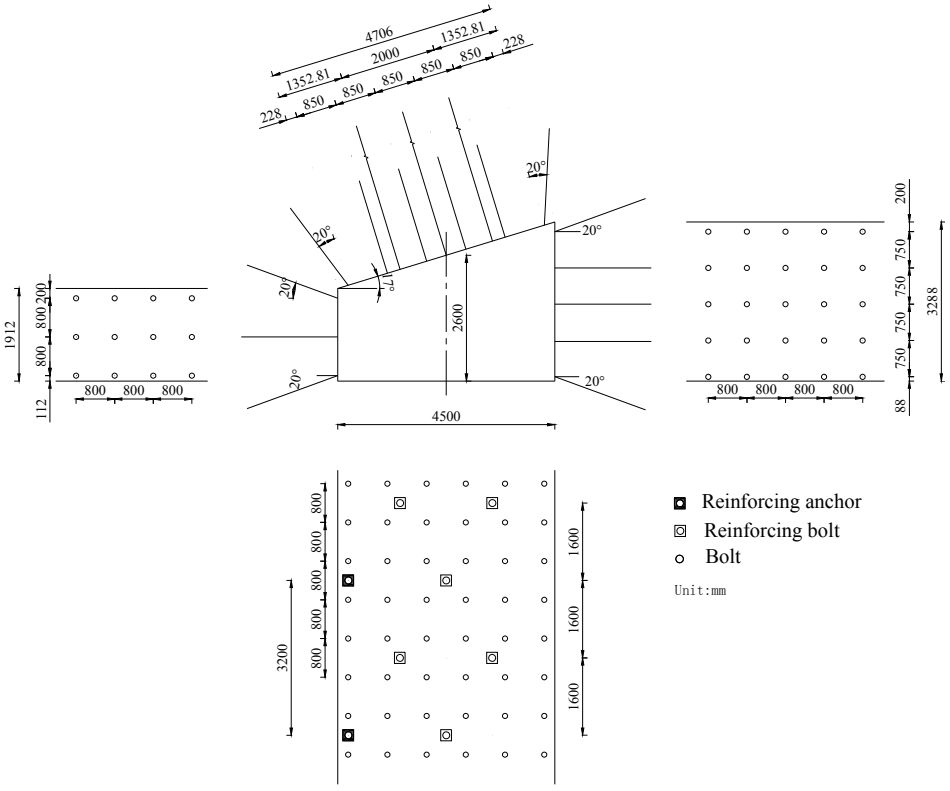

Figure 9. The support arrangement for the roadway in the 72207 working face.

4.1.2. Roadway Strengthening Support

To prevent the excessive deformation of the roadway, hydraulic props and steel beams were installed in the roadway between 120 m behind the working face and 20 m in front of the working face (see Figure 10).

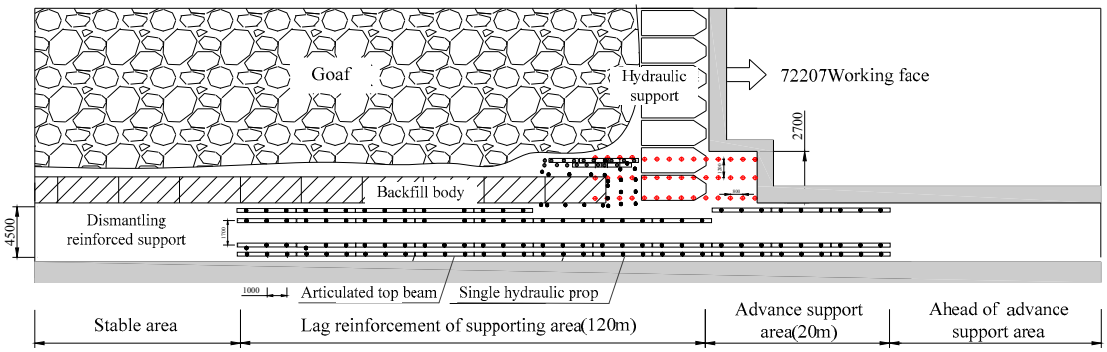

Figure 10. Schematic of strengthening support in gob-side entry retaining.

4.1.3. The Support of A Safe Working Space

In order to ensure smooth backfilling work of the gob-side entry retaining (GER), it is extremely important to keep the roof above the backfill body stable and integrated using shallow-hole blasting to prevent roof separation and fall off. According to the geological conditions, in order to slow down the roof sinking and prevent the backfill body damage before it reaches the preset strength, the roof above the backfill body should be supported. The support scheme is as follows: ensure the safety of the working space in advance by mining the rib close to the working face, and then use bolts (high-strength bolt of $\phi 20 \times 2000$ mm), steel ladder beams, and metal mesh to support the roof above the safe working space. The horizontal width of the safety working space should be 2700 mm, with a depth of 3000–4000 mm. The pitch and row spacing of bolts should be 1200 mm × 800 mm. The support layout is shown in Figure 11.

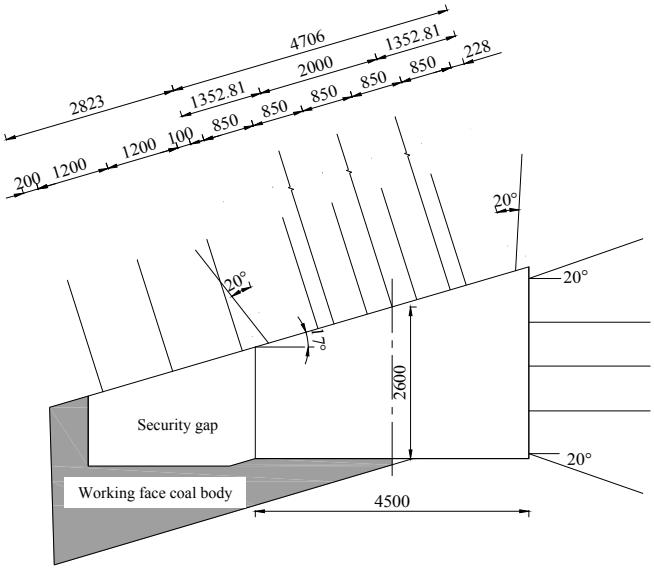

Figure 11. *Cont.*

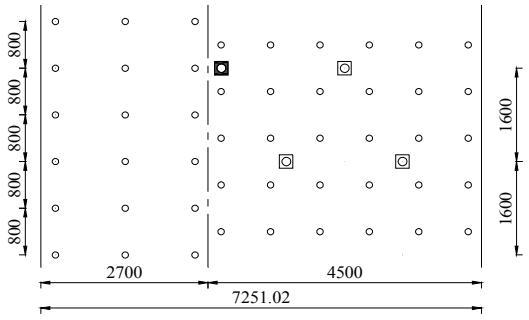

Figure 11. Schematic of safe gap production and support.

4.2. Backfill Body

In order to maintain the maingates, special cement mixtures with the addition of waste are used (fly ash), which increase strength parameters. Super-high-water materials are now widely used to build the backfill body for the gob-side retaining entry in coal mines due to their low cost and high strength. Super-high-water materials use sulfoaluminate cement clinker as the base material and contain gypsum, lime, composite retarder, a suspending agent, and a compound quick-setting agent. The ultimate strength of material at a low water–cement ratio can reach 20 MPa. The strength vs. time relationship of the super-water materials for different water–cement ratios is detailed in Table 5. The water–cement ratio of 1.5: 1 was selected for the backfilling. The width of the backfill body was 1.5 m and its height was the mining height. The backfilling length at one time was 3.2 m.

Table 5. Uniaxial compressive strength of high-water material under different water–cement ratios.

Water Cement Ratio	Cementing Dosage ($kg \cdot m^{-1}$)	Water Dosage ($kg \cdot m^{-1}$)	Gelation Time (min)	Compressive Strength (MPa)			
				2 h	24 h	7 days	28 days
0.8	873	698	7	14.40	19.0	21.32	22.55
1.0	744	744	8	10.2	15.8	17.90	19.10
1.2	647	776	8	8.40	14.0	15.22	16.97
1.5	542	813	10	4.48	9.14	10.36	11.51
2.0	426	850	12	3.33	6.26	7.92	8.70
2.25	385	866	14	2.42	4.74	6.19	7.08
2.5	352	880	16	2.05	3.97	5.08	5.44

Figure 12 schematically shows the reinforcement diagram for the backfill body. In order to improve the resistance of the backfill body to deformation, special rock bolts which can be pretensioned from both ends were placed inside of the filling bag before the addition of the super-high-water materials, as can be seen in Figure 12. Pretensions were applied at both ends of the rock bolts after the backfill body hardened, which could further increase the strength of the backfill body. The rock bolts used in the backfill body were 22 mm in diameter and 1.7 m long. A steel mesh and a beam were also used to reinforce the backfill body. It was concluded that the presented results form the basis for a future longwall for which maingates can be maintained more efficiently.

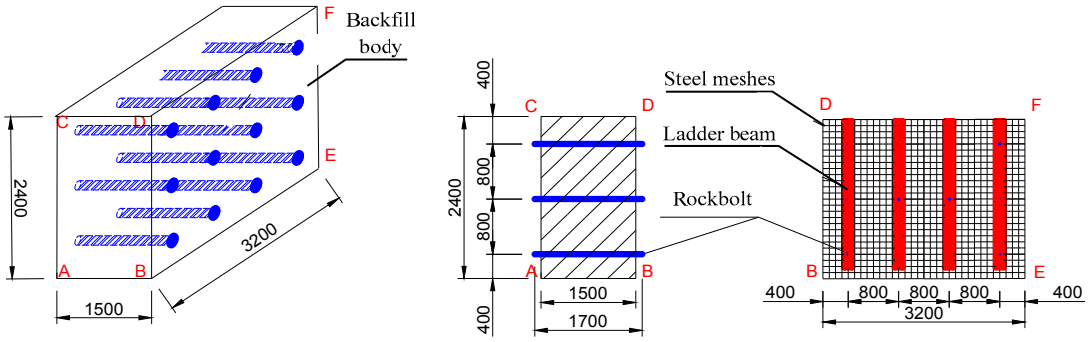

Figure 12. Schematic diagram of reinforcement of backfill body.

4.3. The Design of the Shallow-Hole Blasting

Using the previous research results, a hole depth of 5.0 m was determined and the hole spacing was 1.0 m. The hole direction was designed to incline to the gob area at 10° in order to facilitate cave-in of the roof strata. The distance between the hole and the body was set as 500 mm to avoid damaging the backfill body. Each cumulative tube was loaded with four blasting explosive cartridges, and each borehole had two cumulative tubes. A detonator was installed on the last explosive cartridge. The mud sealing length of the borehole was 2 m.

The specific parameters of the blasting borehole are shown in Table 6, and the borehole layout is shown in Figure 13.

Table 6. Specific parameters of the blasting hole.

Depth of Blasting Hole (m)	Angle (°)	Hole Size (mm)	Explosive Charge in Per Hole		Sealing Mud Length (m)
			Number of Rolls/Branches	Weight (kg)	
5.0	10	42	8	2.4	2.0

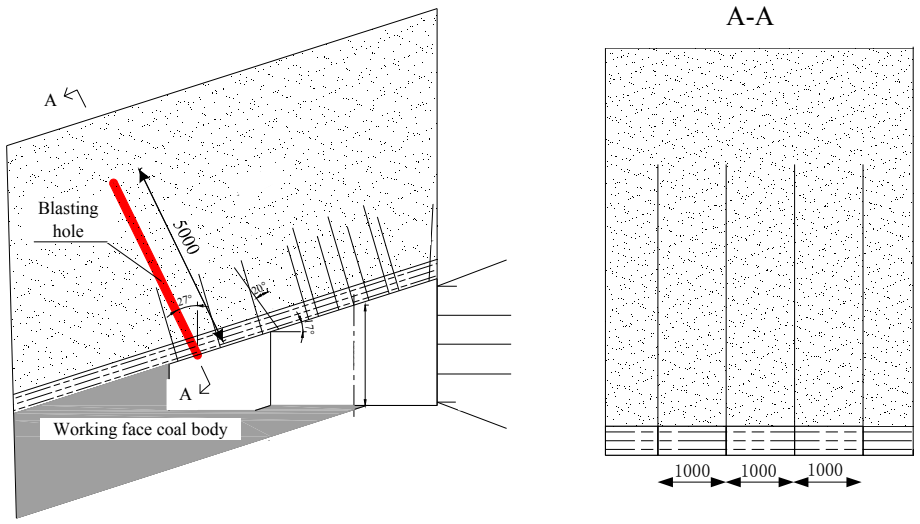

Figure 13. Diagram of shallow-hole blasting hole.

5. Discussions on the Field Measurements

The measured displacement curve of the gob-side retaining entry in the 72207 working face with the application of shallow-hole blasting is shown in Figure 14a. On the other hand, the gob-side retaining entry was also built in the 72201 working face with the same geological conditions and the same supports as the 72207 working face; however, shallow-hole blasting was not carried out in the

72201 working face. Figure 14b shows the deformation of the gob-side retaining entry in the 72201 working face.

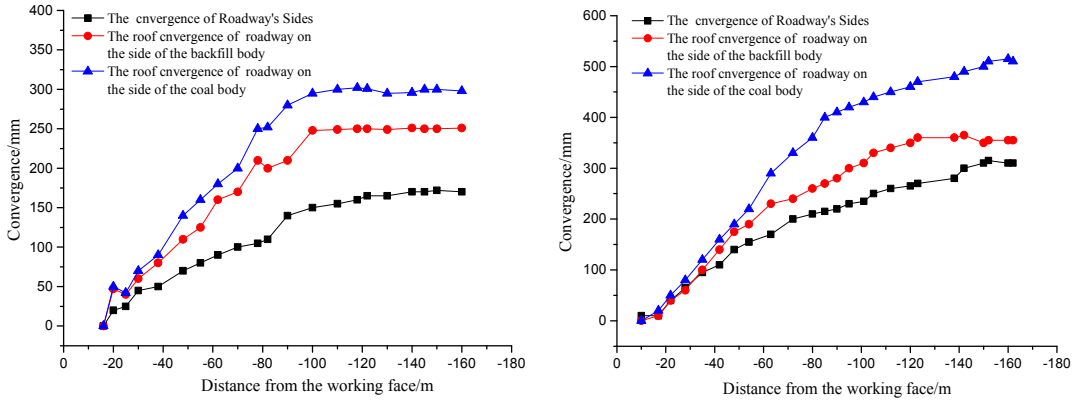

Figure 14. The deformation of the gob-side retaining entries for the 72207 and the 72201 working faces: (**a**) the amount of surrounding rock moving in the 72207 working face rail roadway; (**b**) the amount of surrounding rock moving in the 72201 working face rail roadway.

The roof-to-floor convergence at the side of the solid coal rib was larger than that at the side of the backfill body. The deformation of gob-side retaining entry in the 72207 working face increased quickly in the range of 10–90 m behind the working face. The deformation of surrounding rock mass tended to become stable after 90 m behind the working face. The ultimate roof-to-floor convergence nearby the solid coal rib of the 72207 working face was about 361 mm, the roof-to-floor convergence close to the backfill body was about 292 mm, and the rib-to-rib convergence was 182 mm.

For the 72201 working face without shallow-hole blasting, the entry tended to become stable at 100 m behind the working face. The ultimate roof-to-floor convergence near the solid coal rib was about 507 mm, the roof-to-floor convergence near the backfill body was about 387 mm, and the rib-to-rib convergence was 312 mm. The roof-to-floor convergences near the solid coal rib and near the backfill body, and the rib-rib convergence in the 72207 working face with shallow-hole blasting decreased by 29%, 25%, and 42%, respectively, compared to those in the 72201 working face without shallow-hole blasting, under the same geological conditions and the same supports. Figure 15 shows the comparison of the deformation of the gob-side retaining entries with and without shallow-hole blasting. It can be concluded that the shallow-hole blasting technology can significantly reduce the deformation of the entry.

Figure 15. Comparison of the deformation of the gob-side retaining entry with and without shallow hole blasting: (**a**) with shallow-hole blasting; (**b**) without shallow-hole blasting.

6. Conclusions

The gob-side retaining entry with a hard roof in deep mines often encounters the hanging of the roof strata, which could lead to large roof pressure and dynamic disasters. The shallow-hole blasting technique was introduced to weaken the roof strata and to facilitate its cave-in to the gob. The relevant parameters of shallow-hole blasting were determined using theoretical calculations and a LS-DYNA3D numerical simulation: the hole depth was 5.0 m, the hole spacing was 1.0 m, and the single hole charge was 2.4 kg.

The impacts of shallow-hole blasting on the strata control of deep gob-side retaining entry were investigated by comparing two scenarios in the field: a deep gob-side retaining entry with and without shallow-hole blasting. Shallow-hole blasting was implemented in the gob-side retaining entry in the 72207 working face. The deformation of the gob-side retaining entry was measured. As a comparison, the deformation of the gob-side retaining entry in the 72201 working face under the same geological conditions and the same support was also measured. Shallow-hole blasting was not carried out in the 72201 working face. The roof-to-floor convergences in the side of the solid coal rib and in the side of the backfill body, and the rib-rib convergence in the 72207 working face with shallow-hole blasting decreased by 29%, 25%, and 42%, respectively, compared to those in the 72201 working face without shallow-hole blasting. The comparison of the deformation of the two gob-side retaining entry shows that shallow-hole blasting is able to significantly reduce the deformation of the retaining entry.

The main contribution of this study is that shallow-hole blasting was introduced to weaken the strength of the hanging hard roof in the gob-side retaining entry. The field measurement indicates that this technique is able to significantly decrease the deformation of the retaining entry and maintain its stability. This technique would be quite useful in controlling the stability of entries with hard roof strata subject to large deformation.

Author Contributions: Investigation, Y.C.; data curation and paper writing, S.M.; writing—original draft preparation, S.M.; writing—review and editing, Y.Y.; supervision, N.M.; project administration, J.B. All authors contributed equally to this paper.

Funding: The authors acknowledge the Fundamental Research Funds for the Central Universities (2019XKQYMS63). The support of the Sanhejian coal mine during the field investigation is acknowledged.

Acknowledgments: This project was supported by the China University of Mining and Technology.

Conflicts of Interest: The authors declare no conflicts of interest.

References

1. Sun, H.; Zhao, B. *Surrounding Rock Control of Entry Driven Aong Next Goaf*; China Coal Industry Publishing House: Beijing, China, 1993.
2. Liu, K.; Zhang, X.; Li, J. Practices on gateway retaining along goaf side in thin seam with hard roof. *Coal Sci. Technol.* **2011**, *39*, 17–20.
3. Deng, Y.; Tang, J.; Zhu, X. Industrial test of concrete packing for gob-side entry retained in gently-inclined medium-thickness coal seam. *J. Southwest Jiaotong Univ.* **2011**, *46*, 523–528.
4. Hua, X. Development status and improved proposals on gob-side entry retaining support technology in China. *Coal Sci. Technol.* **2006**, *34*, 78–81.
5. Guo, Y.; Bai, J.; Hou, C. Study on the main parameters of gateside packs in gateways maintained along gob-edges. *J. China Univ. Min. Technol.* **1992**, *21*, 1–11.
6. Bu, T.; Feng, G.; Jia, K. Gateway side backfilling support technology of goaf side gateway in fully mechanized high cutting longwall mining face. *Coal Sci. Technol.* **2010**, *38*, 41–44.
7. Kang, H.; Niu, D.; Zhang, Z. Deformation characteristics of surrounding rock and supporting technology of gob-side entry retaining in deep coal mine. *Chin. J. Rock Mech. Eng.* **2010**, *29*, 1977–1987.
8. Chen, Y.; Bai, J.; Wang, X. Support technology research and application inside roadway of gob-side entry retaining. *J. China Coal Soc.* **2012**, *37*, 903–910.
9. Ma, G.; An, X. Numerical simulation of blasting-induced rock fractures. *Int. J. Rock Mech. Min. Sci.* **2008**, *45*, 966–975. [CrossRef]

10. Xie, W.; Da, J.; Feng, G. Mechanism of controlling surrounding rock around gob-side entry retaining in top-coal caving mining face. *J. Cent. South Univ.* **2004**, *35*, 657–661.
11. Han, C. *Stress Optimization and Structure Stability Control for the Surrounding Rock of Gob-Side Entry Retainin*; China University of Mining and Technology: Xuzhou, China, 2013; pp. 1–4.
12. Wang, M.; Wang, M.; Du, H. Gateway retained technology along goaf of coalmining face with thick and hard roo. *Coal Sci. Technol.* **2013**, *41*, 42–45.
13. Wang, F.; Tu, S.; Yuang, Y. Deep-hole pre-split blasting mechanism and its application for controlled roof caving in shallow depth seams. *Int. J. Rock Mech. Min. Sci.* **2013**, *64*, 112–121. [CrossRef]
14. Ning, J.; Ma, P.; Liu, X. Supporting mechanism of "yielding-supporting" beside roadway maintained along the goaf under hard rocks. *J. Min. Saf. Eng.* **2013**, *30*, 369–374.
15. Hao, F.; Zhou, T.; Jing, Y. Forced roof caving technology and application to goaf-side entry retaining. *Coal Sci. Technol.* **2006**, *34*, 16–24.
16. Gao, K.; Liu, Z.; Liu, J. Application of deep borehole blasting to gob-side entry retaining forced roof caving in hard and compound roof deep well. *Chin. J. Rock Mech. Eng.* **2013**, *32*, 1588–1594.
17. Huang, B.; Liu, C.; Fu, J. Hydraulic fracturing after water pressure control blasting for increased fracturing. *Int. J. Rock Mech. Min. Sci.* **2011**, *48*, 976–983. [CrossRef]
18. Liu, S. Application of pre-splitting blasting hard roof in retaining roadway along gob. *Coal Min. Technol.* **2013**, *18*, 79–81.
19. Sim, Y.; Cho, G.; Song, K. Prediction of Fragmentation Zone Induced by Blasting in Rock. *Rock Mech. Rock Eng.* **2017**, *50*, 2177–2192. [CrossRef]
20. Chen, M.; Hu, Y.; Lu, W. Numerical simulation of blasting excavation induced damage to deep tunnel. *Rock Soil Mech.* **2011**, *32*, 1531–1537.
21. Li, B.; Xu, G.; Wang, W. Numerical simulation of fan-hole blasting-induced rock fracture. *China Min. Mag.* **2014**, *23*, 84–99.
22. Wei, X.; Zhao, Z.; Gu, J. Numerical simulations of rock mass damage induced by underground explosion. *Int. J. Rock Mech. Min. Sci.* **2009**, *46*, 1206–1213. [CrossRef]
23. *State Administration of Work Safety, Coal Mine Safety Regulations*; Coal Industry Press: Beijing, China, 2016.
24. Zhu, Z.; Mohanty, B.; Xie, H. Numerical investigation of blasting-induced crack initiation and propagation in rocks. *Int. J. Rock Mech. Min. Sci.* **2007**, *44*, 412–424. [CrossRef]
25. Zhang, Z.; Wang, L.; Silberschmidt, V. Damage response of steel plate to underwater explosion: Effect of shaped charge liner. *Int. J. Impact. Eng.* **2017**, *103*, 38–49. [CrossRef]